

Lattice parameter and hardness variations resulting from precipitation and misfit accommodation in a particle-reinforced Al–Si–Cu–Mg alloy

M. J. Starink, V. M. F. Abeels and P. van Mourik

Laboratory of Metallurgy, Delft University of Technology, Rotterdamseweg 137, 2628 Al Delft (The Netherlands)

(Received September 23, 1992; in revised form November 17, 1992)

Abstract

Precipitation processes occurring in ageing of Al–20at.%Si–1.5at.%Cu–1.1at.%Mg (ASCM) alloys with and without Al₂O₃ particle reinforcement were studied using X-ray diffraction and hardness measurements. During ageing at 453 K after solid quenching, the Q phase (Al₃Cu₂Mg₈Si₆) precipitates first, followed by the θ phase (Al₂Cu). An optimized heat treatment for the ASCM alloys consists of a short solution treatment at 779 K, followed by water quenching and ageing for 4 h at 453 K. After the peak in hardness has occurred, continued ageing decreases the hardness. This overageing results from coarsening of the Q phase. After heat treatment, the lattice parameters were affected by the misfit effects caused by the difference in the coefficients of thermal expansion between the Al-rich phase, Si-rich phase and Al₂O₃ particles if present. These misfits still existed at room temperature after precipitation was completed. A model assuming ideal plastic behaviour of the matrix describes fairly well the cooling-induced changes in the Si-rich phase lattice parameter. For the cooling-induced changes in the Al-rich phase lattice parameter, there remains a difference between model predictions and measurements.

1. Introduction

The wear resistance of Al alloys can be improved by the introduction of finely dispersed hard particles into the alloy [1, 2]. A fine dispersion of Si particles can be obtained by the rapid solidification of a molten Al alloy with a high Si content [3]. A dispersion of ceramic particles in Al alloys can be obtained via various production routes, *e.g.* by compocasting or by mixing particles with Al alloy powders, followed by extrusion. Metals reinforced by dispersed (ceramic) particles are generally referred to as metal matrix composites (MMCs). Their increased wear resistance, low thermal expansion and improved high temperature strength make MMCs attractive for applications such as in parts of combustion engines.

In this article, the results of a study on ageing after solid quenching of Al–20at.%Si–1.5at.%Cu–1.1at.%Mg (ASCM) alloys with and without 10 vol.% Al₂O₃ particles are presented. These alloys combine the presence of two reinforcing components (Si and Al₂O₃ particles) with the possibility of age hardening of the Al-rich matrix phase. Hence, an appropriate heat treatment is necessary to optimize the mechanical properties at room and elevated temperatures. The presence of dispersed particles in solid-quenched, age-hardenable Al alloys generally affects the kinetics and sequences of precipitation processes, as compared with the corresponding unreinforced alloys [4–6].

Non-isothermal precipitation in solid-quenched ASCM alloys has been studied before [7, 8]. In the present work, isothermal precipitation in solid-quenched ASCM alloys is studied by measuring the lattice parameter variations in the Al-rich phase and the Si-rich phase. Lattice parameter measurements also give information about stresses in the inclusions and in the matrix. Residual stresses in MMCs are important, since they have a significant impact on properties such as yield strength and fracture behaviour [9]. In addition, some hardness measurements were performed.

2. Experimental procedures

2.1. Preparation of specimens

The alloys under investigation were made available by the Japanese firm Showa Denko K.K. The base alloy was rapidly solidified by gas atomization, yielding fine powder (particle sizes range from 1 to 100 μm , with a median size of about 24 μm [10]). The cooling rate during gas atomization is generally about 10^4 – 10^6 K s⁻¹ [3]. Subsequently, the powder was mixed with ceramic Al₂O₃ particles to obtain a mixture with 10 vol.% of ceramic particles. Finally, the mixture and the base alloy powders were extruded at about 670 K into round bars with a diameter of about 20 mm. The composite shows a fairly homogeneous distribution of Al₂O₃ particles. The sizes of the Al₂O₃ particles range

TABLE 1. Compositions of the alloys

Alloy name	Al ₂ O ₃ (vol.%)	Si		Cu		Mg		Fe	
		Alloy (wt.%)	Base (at.%)	Alloy (wt.%)	Base (at.%)	Alloy (wt.%)	Base (at.%)	Alloy (wt.%)	Base (at.%)
ASCM0	—	20.2	19.9	3.47	1.52	0.96	1.10	0.24	0.12
ASCM10	10.4 ^a	16.9	19.6	2.97	1.52	0.77	1.03	0.20	0.11

^aCalculated from measured weight percentages using the densities of the ASCM base alloy (2.67 g cm⁻³) and of α -Al₂O₃ (3.98 g cm⁻³) [11].

from 1 to 6 μm , with an average aspect ratio of about 2 [7]. The Si particles are mainly equiaxed with sizes ranging from about 2 to 10 μm [7].

The chemical compositions of the extruded alloys are presented in Table 1. The alloys are indicated by ASCM0 and ASCM10, where the number refers to the volume percentage of Al₂O₃ particles. The main impurities in the base alloy (as measured by X-ray fluorescence) are Ni (about 0.02 at.%), Zn (about 0.01 at.%), Ti (about 0.006 at.%) and Cr (about 0.005 at.%).

From the centre of the extruded bars, cylindrical specimens were machined with a diameter of 0.5 mm and length of about 5 mm. The axis of the specimen was parallel to the extrusion direction. These specimens were intended for X-ray diffraction experiments with a Debye-Scherrer camera.

The specimens were solution treated for 10 min at 779 ± 2 K in a vertical tube furnace and subsequently quenched in water at room temperature. This heat treatment is designated as solid quenching (SQ). The solution treatment temperature is just below the start of melting of the ASCM alloy [7] and equals the solution treatment temperature for the conventional, monolithic 2014 Al alloy, which has a composition comparable with the matrix of the ASCM alloy. (The term matrix indicates the alloy excluding the Si and Al₂O₃ particles.) The quenched specimens were aged at 453 K. (The quenched and aged specimens will be indicated as SQ + A specimens.) The ageing treatment was performed in an oil bath with temperature stability within ± 1.5 K and was interrupted after certain intervals by a direct quench into water at room temperature.

2.2. X-ray diffraction

For measurement of the lattice parameter of the Al-rich phase and the Si-rich phase of the ASCM alloys, X-ray diffraction experiments were performed using a Debye-Scherrer (DbS) camera. Copper radiation filtered by Ni was used. The films in the DbS camera were exposed for 6 h. During the exposure, the temperature inside the DbS camera, at a point close to the specimen, was measured and recorded. The temperatures during the measurements were between 294 and

297 K. Temperature variations during single experiments were typically of the order of 0.5 K. The film type and film development procedures were identical for all the experiments.

After the development of the DbS film, the line positions were measured. The accuracy of the line position measurements of the three lines corresponding to the highest diffraction angle was improved by taking the average of at least five determinations of the position. The lattice parameters of the Al-rich phase and the Si-rich phase were determined using the so-called Nelson-Riley extrapolation (see ref. 12). Reported error values represent the standard deviation resulting from the determination of the lattice parameters using this extrapolation method. The lattice parameters determined by the Nelson-Riley extrapolation were corrected for the average temperature during the measurement by adopting for the coefficient of thermal expansion of pure Al and pure Si the values $23.5 \times 10^{-6} \text{ K}^{-1}$ and $3 \times 10^{-6} \text{ K}^{-1}$ respectively [13]. All the lattice parameters presented in this work are valid at 298 K.

2.3. Hardness measurements

Hardness measurements were performed on the ASCM0 and ASCM10 specimens. The microhardness was measured on polished longitudinal sections using a Leitz-Durimet Vickers hardness tester with an indentation force of 0.981 N. For each hardness value, at least 10 indentations evenly distributed over the polished surface were made. The indentation (about 30 μm in diameter) always covered several Si and Al₂O₃ particles. Irregularly shaped indentations were discarded. The values presented reflect the average of the regularly shaped indentations and the error represents the standard variation.

3. Results

3.1. X-ray diffraction

In all the X-ray diffraction experiments on the ASCM0 and ASCM10 alloys, lines diffracted from the

Al-rich phase, the Si-rich phase, the Q ($\text{Al}_5\text{Cu}_2\text{Mg}_8\text{Si}_6$) phase and the $\text{Al}_7\text{Cu}_2\text{Fe}$ phase were detected. These four phases are equilibrium phases in the ASCM0 alloy (see, for example, refs. 8 and 14). For the ASCM10 alloy, the $\alpha\text{-Al}_2\text{O}_3$ (corundum) phase was also detected. For both the ASCM0 and ASCM10 alloys, lines diffracted by the θ phase appeared after 4 h of ageing after solid quenching. Except these six phases, no other phases were detected during isothermal ageing of the SQ ASCM0 and ASCM10 alloys. Directly after SQ, the Al-rich phase lattice parameters of the ASCM0 and ASCM10 alloys are 0.40463 ± 0.00004 nm and 0.40473 ± 0.00003 nm respectively. The Al-rich phase lattice parameters of the ASCM0 and ASCM10 alloys during ageing at 453 K after SQ are given in Fig. 1. In the initial stage of ageing, the Al-rich phase lattice parameters of both the ASCM0 and the ASCM10 alloys remain approximately constant. Between 2 and 32 h of ageing, the lattice parameters of both alloys increase to reach a value which remains approximately constant during prolonged ageing. This stationary value is higher than the lattice parameter of pure unstrained Al (0.40496 nm [15]).

Directly after SQ, the Si-rich phase lattice parameters of the ASCM0 and ASCM10 alloys are 0.54295 ± 0.00008 nm and 0.54283 ± 0.00004 nm respectively. In Fig. 2, the Si-rich phase lattice parameters of the ASCM0 and the ASCM10 alloys during ageing at 453 K are presented. The Si-rich phase lattice parameters of both alloys are significantly lower than the lattice parameter of pure unstrained Si (0.54308 nm [16]). The Si-rich phase lattice parameters of the two alloys do not differ significantly and remain approximately constant during ageing.

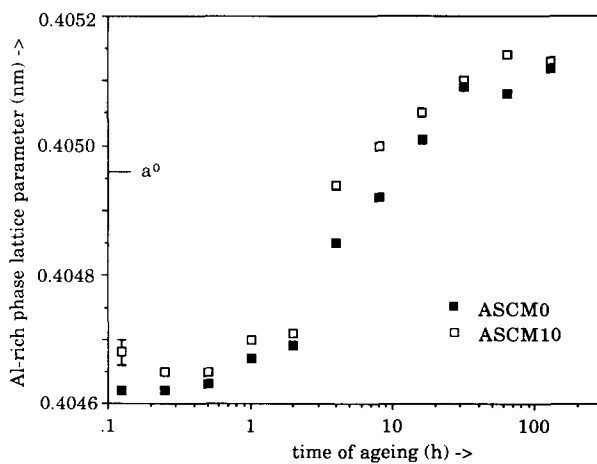


Fig. 1. Al-rich phase lattice parameters of the ASCM0 (■) and ASCM10 (□) alloys as a function of ageing time at 453 K. The lattice parameter for pure aluminium (a_{Al}^0) is indicated. Typical standard deviation is indicated.

3.2. Hardness measurements

The hardness of the ASCM0 and the ASCM10 alloys as a function of time of ageing at 453 K is shown in Fig. 3. The standard deviations of the hardness values in the 10 separate indentations for each ageing time are on average 5 HV for the ASCM0 specimen and 10 HV for the ASCM10 specimen. The higher standard deviation for the ASCM10 specimen is probably due to small variations in the local density of Al_2O_3 particles. It is observed that the hardness of the ASCM10 alloy is always significantly higher than the hardness of the ASCM0 alloy. During artificial ageing, the difference is on average 28 HV and remains approximately constant. After quenching from the solution treatment temperature, the difference is 42 HV. For both alloys, the time to reach the peak hardness is 4 h. The peak hardness is 187 HV for the ASCM0 alloy and 217 HV for the ASCM10 alloy. For the ASCM0 alloy, the peak hardness value equals that obtained during non-isothermal ageing at a heating rate

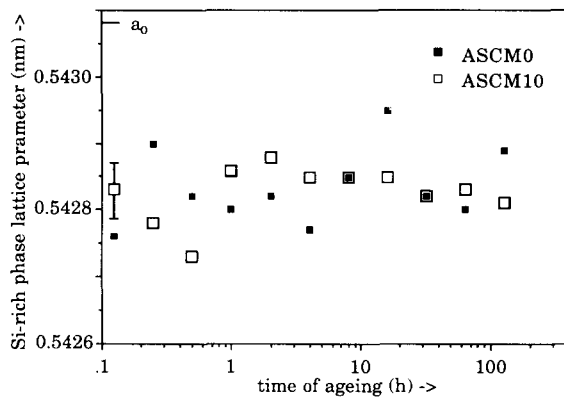


Fig. 2. Si-rich phase lattice parameter of the ASCM0 (■) and ASCM10 (□) alloys as a function of ageing time at 453 K. The lattice parameter for pure silicon (a_{Si}^0) is indicated. Typical standard deviation is indicated.

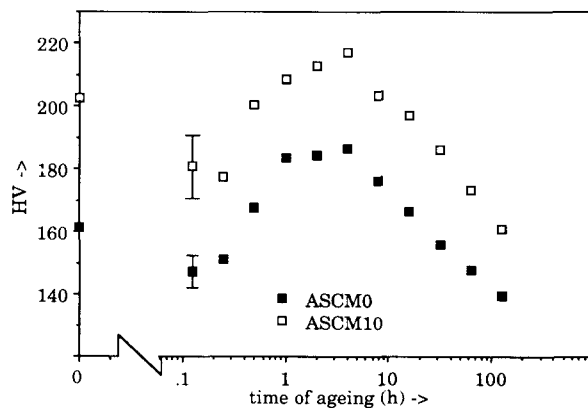


Fig. 3. Vickers microhardness HV of the ASCM0 (■) and ASCM10 (□) alloys during ageing at 453 K after solid quenching. Typical standard deviations are indicated.

of 2 K min^{-1} [7]. It is noted that all the hardness values measured during ageing after SQ are appreciably higher than the hardness of the as-extruded ASCM0 alloy (107 HV [7]).

4. Lattice parameter changes owing to dissolved atoms and misfitting inclusions

For an Al-based composite in which alloying atoms can dissolve in the Al-rich phase, two types of effect contribute to the deviation of the Al-rich phase lattice parameter from the lattice parameter of pure Al: the shift owing to dissolved atoms and the shift owing to misfitting inclusions.

4.1. Lattice parameter changes owing to dissolved atoms

In binary Al-Cu and Al-Si alloys, alloying atoms dissolved in the Al-rich phase decrease the lattice parameter of the Al-rich phase. In both alloys, the lattice parameter shift is proportional to the amount of dissolved atoms. In Al-Mg alloys, dissolved Mg atoms increase the Al-rich phase lattice parameter. For high Mg contents of the Al-rich phase (greater than 2 at.% Mg), the effect increases linearly with the Mg content of the Al-rich phase. For low Mg contents, a non-linear dependence of the Al-rich phase lattice parameter on the Mg content is observed (see Fig. 4).

In many ternary alloy systems the lattice parameter change in the Al-rich phase owing to two different elements being dissolved is in good approximation equal to the sum of the two independent contributions [20]. Then, the interaction between the two types of solute atom can be neglected and the lattice parameter shifts can be obtained from the lattice parameter shifts in the binary alloy systems. In Al-Cu-Si alloy, the

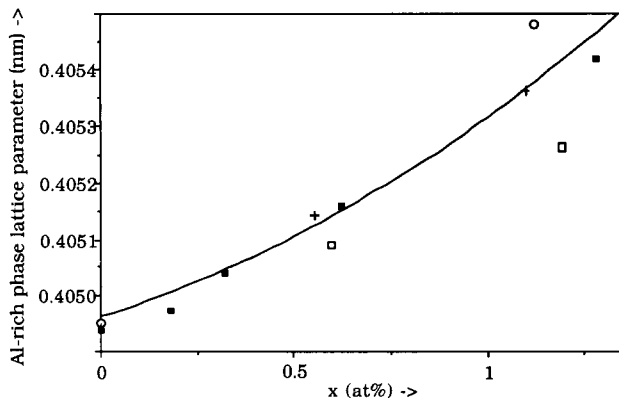


Fig. 4. Al-rich phase lattice parameters of Al-Mg alloys. Data from refs. 17 (\square), 18 (+), 19 (\circ) and 22 (\blacksquare). The curved line represents the Al-rich phase lattice parameter as a function of its Mg content, as used in the present work.

interaction is negligible [16]. In Al-Mg-Si alloys with 0.72–1.42 at.% of alloying elements dissolved in the Al-rich phase, significant contractions of the Al-rich phase owing to solute-solute interactions were observed [21]. The lattice parameter shift owing to solute-solute interactions reaches its maximum for the quasi-binary composition associated with the Mg_2Si phase. Hill and Axon [21] suggested that the interaction term Δa^i can be approximated by

$$\Delta a_{\text{Mg-Si}}^i = -[\text{Mg}_2\text{Si}] \times 0.026 \text{ nm} \quad (1)$$

where $[\text{Mg}_2\text{Si}]$ is the virtual concentration of Mg_2Si in the Al-rich phase, *i.e.* $[\text{Mg}_2\text{Si}] = \frac{1}{2}[\text{Mg}]$ when $[\text{Mg}] < 2[\text{Si}]$ or $[\text{Mg}_2\text{Si}] = [\text{Si}]$ when $[\text{Mg}] \geq 2[\text{Si}]$. Also, in Al-Cu-Mg alloys, contractions owing to solute-solute interactions occur [22]. The data are too scarce and the uncertainties in the individual points too large to obtain the dependence on the Cu and Mg fractions of the Al-rich phase. However, the interactions are very small (maximum shift about 0.00006 nm for Al-(1-x)at.%Cu-2xat.%Mg alloys, where x is of the order of 0.25–0.5 [22]). It is assumed that, for the Mg-Cu interactions, a relationship analogous to that for Mg-Si interactions holds. In the case of Cu-Mg interactions, it is assumed that the interactions are proportional to the virtual concentration of S (Al_2CuMg) phase. Consequently, the maximum lattice parameter shift for the Al-(1-x)at.%Cu-2xat.%Mg alloys studied by Poole and Axon [22] should be observed for $x = \frac{1}{3}$, *i.e.* for Al- $\frac{2}{3}$ at.%Cu- $\frac{2}{3}$ at.%Mg. This is in fair agreement with their results. As the maximum shift found by them equalled 0.00006 nm, it is found that

$$\Delta a_{\text{Cu-Mg}}^i = -[\text{Al}_2\text{CuMg}] \times 0.009 \text{ nm} \quad (2)$$

To our knowledge, no data on the lattice parameters of the Al-rich phase in the quaternary Al-Cu-Mg-Si system are available. However, neglecting interactions between Cu, Mg and Si, lattice parameter changes in the Al-rich phase in the ASCM alloy owing to dissolved atoms (Δa_{Al}^d) are obtained from

$$\frac{\Delta a_{\text{Al}}^d}{a_{\text{Al}}^o} = p_{\text{Si}}x_{\text{Si}} + p_{\text{Cu}}x_{\text{Cu}} + p_{\text{Mg}}(x_{\text{Mg}}) + \frac{\Delta a_{\text{Cu-Mg}}^i + \Delta a_{\text{Mg-Si}}^i}{a_{\text{Al}}^o} \quad (3)$$

where x_{Cu} and x_{Si} are the concentrations of Cu and Si atoms in the Al-rich phase, p_{Si} and p_{Cu} are the Vegard constants describing the effects of dissolved Si and Cu atoms on the Al-rich phase lattice parameter in the binary alloys (-4.30×10^{-2} and -1.18×10^{-1} respectively [16]), and $p_{\text{Mg}}(x_{\text{Mg}})$ is the non-linear function which describes the effect of dissolved Mg atoms on the Al-rich phase lattice parameter (see Fig. 4).

4.2. Lattice parameter changes owing to misfit accommodation

When a multiphase alloy is subjected to temperature changes, misfit stresses will be introduced, owing to differences in the coefficients of thermal expansion (CTEs) of the phases. These misfit stresses include a hydrostatic component which changes the lattice parameters of both the matrix and the misfitting inclusions. A model for the lattice parameter changes owing to misfit accommodation in a matrix alloy with spherical misfitting particles was presented earlier [16]. As both the Si and the Al_2O_3 particles in the ASCM alloys are approximately equiaxed [7], this model is used to describe the stress state of these alloys. In the model, the matrix is assumed to be a perfectly plastic material (non-strain hardening), the flow stress-strain behaviour is assumed to be independent of the strain rate and stress orientation, and both the inclusion and matrix are assumed to be isotropic. These assumptions lead to the following expressions for the hydrostatic component p^{im} of the stresses in the elastically deforming zone of a spherical matrix A (radius R) with a spherical inclusion B in its centre:

$$p^{\text{im}} = -p_{\text{B}} - 2\sigma_{\text{y}} \ln\left(\frac{R}{a}\right) \quad R \leq r_{\text{p}} \quad (4a)$$

$$p^{\text{im}} = \frac{2}{3} \sigma_{\text{y}} \left(\frac{r_{\text{p}}}{R}\right)^3 \quad R \geq r_{\text{p}} \quad (4b)$$

where σ_{y} is the yield strength of the matrix, r_{p} is the radius of the plastic zone, p_{B} is the internal pressure (the difference between the pressure in the inclusion and p^{im}) and a is the radius of the inclusion. The volume fraction y_{B} of inclusions is given by

$$y_{\text{B}} = \left(\frac{a}{R}\right)^3 \quad (5)$$

and r_{p} and p_{B} can be obtained from

$$r_{\text{p}} = a \exp\left(-\frac{p_{\text{B}}}{2\sigma_{\text{y}}} - \frac{1}{3}\right) \quad (6)$$

$$\frac{6\eta\mu_{\text{A}}\varepsilon}{\sigma_{\text{y}}}\left(1 + \frac{p_{\text{B}}}{3K_{\text{B}}\varepsilon} - \frac{p_{\text{B}}}{3K_{\text{A}}\varepsilon}\right) = \exp\left(-\frac{3p_{\text{B}}}{2\sigma_{\text{y}}} - 1\right) \quad (7)$$

where μ_{A} is the shear modulus, K_{A} and K_{B} are the respective bulk moduli, $\eta = (1 + \nu_{\text{A}})/3(1 - \nu_{\text{A}})$ (where ν_{A} is Poisson's constant for the matrix) and ε is the linear misfit parameter. For the misfit ε_{T} introduced by the thermal expansion mismatch, it holds that

$$\varepsilon_{\text{T}} = \Delta\alpha \Delta T \quad (8)$$

where $\Delta\alpha$ is the difference in CTE between the matrix and reinforcement, and ΔT is the temperature change

applied. For the case in which the bulk modulus of the inclusions deviates from the bulk modulus of the matrix, the hydrostatic component of the misfit stress (often termed the image stress) also contributes to the misfit. This contribution is given by

$$\varepsilon_{p^{\text{im}}} = p^{\text{im}}(K_{\text{B}}^{-1} - K_{\text{A}}^{-1})/3 \quad (9)$$

(It should be noted that for Si and Al_2O_3 inclusions in an Al matrix $K_{\text{B}} > K_{\text{A}}$ and $\Delta\alpha > 0$. Hence, ε_{T} and $\varepsilon_{p^{\text{im}}}$ are of opposite sign.) This effect is limited for the case of Si particles in an Al-rich matrix, since the bulk moduli of the two phases are of the same order of magnitude. Because of the high bulk modulus of the Al_2O_3 particles, this effect can be important for Al_2O_3 particles in an Al-rich matrix.

The model presented above was derived for one single type of misfitting inclusion. In the ASCM10 alloy, both Si and Al_2O_3 particles are present. To obtain the image stress for this case, we will use an iteration method similar to that suggested by Hamann *et al.* [23] for elastic accommodation in a composite containing various types of misfitting inclusion. This iteration consists of the following steps.

Zeroth order. Assume $\varepsilon = \varepsilon_{\text{T}}$ and calculate p_{B} , r_{p} and p^{im} for each type of inclusion (j) separately. Denote the image-stress-induced inclusions of type j in the zeroth order by $(p^{\text{im}})^{j,0}$. Then take

$$p^{\text{im},0} = \sum_j (p^{\text{im}})^{j,0}$$

kth order. Assume $\varepsilon = \varepsilon_{\text{T}} + \varepsilon_{p^{\text{im}}}$ with p^{im} approximated by $p^{\text{im},k-1}$ and calculate p_{B} , r_{p} and p^{im} for each type of inclusion (j) separately. Denote the image-stress-induced inclusions of type j in the k th order by $(p^{\text{im}})^{j,k}$. Then take

$$p^{\text{im},k} = \sum_j (p^{\text{im}})^{j,k}$$

For the case of Si and Al_2O_3 particles in an Al-rich matrix, this method converges rapidly (second-order corrections are smaller than 1%).

Neglecting the lattice parameter of the plastically deformed zone, the lattice parameter change in the matrix owing to misfit stresses ($\Delta a_{\text{A}}^{\text{m}}$) is given by

$$\frac{\Delta a_{\text{A}}^{\text{m}}}{a_{\text{A}}} = \frac{p^{\text{im}}}{3K_{\text{A}}} \quad (10)$$

For the inclusion, it holds that

$$\frac{\Delta a_{\text{B}}^{\text{m}}}{a_{\text{B}}} = \frac{p_{\text{B}} + p^{\text{im}}}{3K_{\text{B}}} \quad (11)$$

The contribution of misfitting θ - and θ' -phase particles to the total lattice parameter change is about one

order of magnitude lower than the contribution of misfitting Si particles to the lattice parameter change [16]. Therefore, the misfit around θ - and θ' -phase particles is neglected. The CTE of the Q phase is not known. However, since in the ASCM alloys the amount of Q phase formed is much lower than the amount of Si phase (see Appendix A), the effect of misfitting Q-phase particles on misfit stresses is much smaller than the effect of misfitting Si-phase particles. For this reason, the contribution of misfitting Q-phase particles to p^{im} is also neglected. Hence, only two types of particle causing significant misfit strains are considered: Si particles and Al_2O_3 particles.

A problem in the evaluation of the eqns. (4)–(11) for the misfit stresses is the anisotropy of Al, Si and Al_2O_3 . The theory described above predicts that the inclusions are in a state of uniform hydrostatic stress. In that case, the strains in the Si particles are determined solely by the S_{11} and S_{12} elastic compliances. The interaction of stress fields and the anisotropy of the phases in the ASCM alloys will cause deviations from the purely hydrostatic stress state in the inclusions. However, providing that these disturbances are small, it is still justified to obtain the elastic constants of the Si inclusions from the S_{11} and S_{12} compliances. Since misfitting $\alpha\text{-Al}_2\text{O}_3$ particles in an Al matrix are nearly incompressible (the bulk modulus of $\alpha\text{-Al}_2\text{O}_3$ is 350 GPa, which is about five times that of Al), the dependence of the elastic constants on the crystallographic directions does not affect the strains in the matrix very much and, in this work, $\alpha\text{-Al}_2\text{O}_3$ is assumed to be isotropic (Young's modulus is estimated by the value for polycrystalline Al_2O_3 as given by Crandall *et al.* [24], while ν is estimated to equal $-S_{12}/S_{11}$, as given by Tefft [25]). The anisotropy of Al is relatively small. For this reason, the elastic constants of polycrystalline Al are used for the calculations. The yield strength of the matrix around the Si and Al_2O_3 particles in the initial part of ageing (up until about 0.5 h) is estimated to equal the yield strength of the 2014 Al alloy (approximate composition Al-2at.%Cu-1.5at.%Mg-1at.%Si) aged for a few minutes at 450 K subsequent to homogenizing and quenching (250 MPa [26]). Since the hardness of the overaged ASCM alloy approximately equals the hardness of the alloy in the

initial state of ageing (see Section 3.2), the yield strength of the matrix in the overaged state is also estimated as 250 MPa. The material constants used are gathered in Table 2.

5. Discussion

5.1. Lattice parameter changes in the ASCM alloys during ageing

To apply eqns. (1)–(3) to the solid-quenched alloys, the composition of the Al-rich phase at that stage should be known. The calculation of the composition of the Al-rich phase after SQ, using the quaternary Al-Cu-Mg-Si phase diagram, is outlined in Appendix A. After SQ, the fraction of Al-rich phase in the base alloy equals 0.78. The composition of the Al-rich phase in the solid-quenched ASCM alloys is estimated to be Al-1.5at.%Cu-0.7at.%Mg-0.5at.%Si.

From eqn. (3), it follows that, for the formation of Q phase in its stoichiometric composition, the effects of Cu, Mg and Si precipitation on the Al-rich phase lattice parameter approximately balance. Therefore, Q-phase formation does not change the Al-rich phase lattice parameter. It is also apparent that θ -phase formation, which involves the precipitation of Cu from the Al-rich phase, increases the Al-rich phase lattice parameter. The formation of Q and θ phases can account fully for the lattice parameter changes during ageing. As was also observed during non-isothermal ageing of solid-quenched ASCM alloys, Q-phase precipitates are the first phase to form. During Q-phase formation, the lattice parameter remains approximately constant, while the hardness increases (see Figs. 1 and 4). The hardness increase during Q-phase formation was also observed during non-isothermal ageing of the same alloy [7]. The next phase to precipitate is the θ phase, causing an increase in the Al-rich phase lattice parameter. This increase starts after between 2 and 4 h of ageing (see Fig. 1). This corresponds well with the appearance of θ -phase lines after 4 h of ageing. The precipitation of θ phase does not increase the hardness [14], as is indeed observed (see Fig. 3). On prolonged ageing (over 4 h), Q-phase precipitates will coarsen and overageing occurs (see next section).

Besides dissolving alloying atoms, also misfit accommodation is expected to affect the lattice parameter of the Al-rich phase. Computation of misfit stresses in a two-dimensional Al-based composite by the finite-element method indicates that a disturbance of the average macrostress at the surface occurs in a layer about $7\ \mu\text{m}$ thick [27]. The penetration depth of X-rays in Al is much larger and the effect of surface relaxation on the stresses determined by X-ray diffraction is about 2% [27]. Considering the accuracy of our

TABLE 2. Elastic constants, yield strength and coefficients of thermal expansion used

	α ($\times 10^{-6}\ \text{K}^{-1}$)	K (GPa)	μ (GPa)	σ_y (MPa)
Matrix ASCM	23.5	69	27	250
Si	3.0	99	51	—
Al_2O_3	7.1	350	156	—

measurements, the surface relaxation of stresses is negligible.

In Table 3, the hydrostatic pressure p_B on misfitting Al_2O_3 and Si particles in an infinite matrix and the image stresses, as obtained from eqns. (4)–(9), are given for the applied temperature changes ΔT . In the same table, the predicted lattice parameter changes owing to misfit stresses are compared with the experimentally observed changes. The strains in the Al-rich phase are obtained from the Al-rich phase lattice parameters for the three longest ageing times (see Fig. 1), where precipitation is thought to be completed (see second paragraph of this section). (The equilibrium solid solubilities at 453 K (see Appendix A) cause a relative lattice parameter shift of about -0.3×10^{-4} . The experimentally observed lattice parameters in the final stages of ageing are corrected for this shift.) Directly after SQ and in the first stage of ageing, the effects of dissolved atoms on the Al-rich phase lattice parameter are much larger than the effect of the image stress. Because of the large uncertainties involved in the determination of the effect of dissolved atoms on the Al-rich phase lattice parameter, any correction for this effect will be prone to large errors. Hence, no attempt was made to obtain the contribution of the misfit stresses to the lattice parameter shifts directly after SQ. From Table 3, the following observations can be made.

(1) The Si-phase lattice parameter shifts after quenching from the ageing temperature, as predicted by the model ($-6a_{\text{Si}}^0 \times 10^{-4}$ for ASCM0 and $-5.4a_{\text{Si}}^0 \times 10^{-4}$ for ASCM10), are somewhat larger than the measured shifts but are within the range of observed lattice parameter shifts (see Fig. 2). Models considering only elastic accommodation predict even larger values for the Si-phase lattice parameter shift (about $-7a_{\text{Si}}^0 \times 10^{-4}$). After quenching from the solution treatment temperature, the correspondence between the measurements and model predictions is limited. (It should be noted that if pure elastic accom-

modation is assumed, after quenching from the solution treatment temperature, the discrepancy between the theoretical predictions and experimental results also would be much larger.)

(2) Both the experimental values and theoretical predictions indicate that the Al-rich phase lattice parameter shift after quenching from the ageing temperature is higher for the ASCM10 alloy as compared with the ASCM0 alloy. The observed difference between the two shifts is predicted fairly well by the theory.

(3) For the Al-rich phase, there exists a difference between the misfit stresses predicted by the model and those measured. Since the misfit stresses predicted by the model are relatively insensitive to variations in the yield stress and elastic constants [16], it is highly unlikely that inaccurate values for these parameters can explain this difference.

For several other Al-based composites, the predictions of Eshelby-type models for the stress in matrices owing to elastic misfit accommodation are also lower than the measured stresses [16, 28–30]. The application of the von Mises yielding criterion [16] indicates that plastic accommodation occurred for the cases reported. Since the present model for elastic–plastic accommodation of misfitting spherical inclusions in a finite matrix gives shifts in the Al-rich phase lattice parameter which are smaller than those in the case of purely elastic accommodation, the predicted stresses for the case of elastic–plastic accommodation will be lower than the measured stresses.

Another striking observation is that, for the ASCM0 specimens, and also for a largely similar Al-20at.%Si-1.3at.%Cu alloy [16], the measured average stress $\langle\sigma_B\rangle$ in the inclusion and the average stress $\langle\sigma_A\rangle$ in the Al-rich phase do not satisfy the rule for the equilibrium of forces in a two-phase system:

$$(1 - y_B)\langle\sigma_A\rangle + y_B\langle\sigma_B\rangle = 0 \quad (12)$$

TABLE 3. Hydrostatic pressure p_B on misfitting Al_2O_3 and Si particles in an infinite matrix and the image stresses p^{im} , as obtained from eqns. (4)–(9) for two temperature drops ΔT

ΔT (K)	Theoretical values			$\Delta a_{\text{Si}}/a_{\text{Si}}$		$\Delta a_{\text{Al}}/a_{\text{Al}}$	
	$p_B(\text{Al}_2\text{O}_3)$ (MPa)	$p_B(\text{Si})$ (MPa)	p^{im} (MPa)	Theory ($\times 10^{-4}$)	Experiment ($\times 10^{-4}$)	Theory ($\times 10^{-4}$)	Experiment ^a ($\times 10^{-4}$)
ASCM0							
160	—	–233	55	–6.0	–4.6	2.7	4.0
486	—	–412	160	–8.4	–2.4	7.7	—
ASCM10							
160	–214	–232	71	–5.4	–4.3	3.4	4.5
486	–382	–411	203	–7.0	–4.6	9.8	—

^aThe experimental values for a_{Al} are corrected for the effect owing to dissolved atoms.

The apparent failure to satisfy the rule for equilibrium of forces also has been observed for Al-SiC composites studied by neutron diffraction [31]). An explanation for this, and for the differences between the theory and experiments noted in the two previous paragraphs, might be an increase in the volume of the plastic zone owing to the creation of defects, such as dislocations and vacancies [16].

5.2. Effect of heat treatment on the hardness

The average dislocation density of a heat-treated MMC increases with the volume fraction of reinforcement [32, 33], while the subgrain size generally decreases with increasing volume fraction of reinforcement [34, 35]. Both these effects increase the yield strength of the composite with increasing volume fraction. The increase in yield strength ($\Delta\sigma_y$) owing to an increase in dislocation density ρ can be estimated from [36]

$$\Delta\sigma_y = A\mu b\rho^{1/2} \quad (13)$$

where b is the Burgers vector in Al (0.286 nm) and A is a constant (usually taken as 1.25) [36]. The average dislocation density in the matrix owing to misfitting inclusions has been estimated by various workers. The general expression is [37–39]

$$\rho = By_B\varepsilon/\{bd(1 - y_B)\} \quad (14)$$

where d is the smallest dimension of the particle and B is a numerical constant which depends on the shape of the misfitting inclusion. Different methods for the evaluation of B have been proposed. According to Arsenault and Shi [37], who considered the minimal amount of dislocations necessary to accommodate a rectangular particle, B varies between 4 for particles elongated in one direction and 12 for equiaxed particles. For incompressible spherical particles, Dunand and Mortensen [39] obtained $B = 12(2^{1/2})$. As the particles present in the alloys most resemble the latter case, the latter value for B is adopted. The yield strength of an Al alloy is usually proportional to its hardness [40]. From a comparison of hardness measurements with tensile tests performed previously on the ASCM alloys [7, 41], it appears that

$$\sigma_y \text{ (MPa)} = 2.1 \text{ HV} \quad (15)$$

Using eqns. (13)–(15), the hardness increase caused by dislocations introduced by thermal misfit can be calculated. For the ASCM0 and ASCM10 alloys, this yields hardness differences of 14 HV after ageing at 453 K and 24 HV after quenching from the solution treatment temperature.

The subgrain structure of the ASCM alloys also can have a significant effect on the hardness [34]. Arsenault *et al.* [35] measured subgrain sizes and dislocation den-

sities in 1100 and 6061 Al alloys reinforced with SiC particles produced by powder metallurgy routes. They showed that, for a volume fraction of inclusions of about 20 vol.% with sizes of the order of 1 μm , the strengthening effect owing to subgrains roughly equals the strengthening resulting from dislocation generation. Applying this result to the alloys studied, the hardness differences owing to dislocation and subgrain strengthening between the ASCM10 alloy and the ASCM0 alloy are estimated at 28 HV and 48 HV after artificial ageing and after quenching from solution treatment temperature respectively. These values agree fairly well with the observed hardness differences: 28 HV and 42 HV (see Section 3.2).

On continued ageing after reaching the peak hardness, the hardness decreases. This hardness decrease is expected to be caused by coarsening of Q-phase precipitates. According to Shercliff and Ashby [42], the mean particle radius r_m at time t_e is related to the radius r_0 at time t_0 according to

$$r_m^3 - r_0^3 = A_1 \int_{t_0}^{t_e} \frac{E_A}{kT} \exp\left(-\frac{E_A}{kT}\right) dt \quad (16)$$

where k is Boltzmann's constant, t is the time, E_A is the activation energy for coarsening and A_1 is a constant. Thus, the state of the coarsening process depends on a temperature corrected time β such that

$$\beta = \int_{t_0}^{t_e} \frac{E_A}{kT} \exp\left(-\frac{E_A}{kT}\right) dt \quad (17)$$

According to the classical Lifshitz-Slyozov-Wagner (LSW) coarsening theory [43, 44] the rate of coarsening in a binary system is proportional to the product of the solubility and the diffusion rate. Extensions and modifications of this theory which account for a non-zero volume fraction of coarsening particles (the original LSW coarsening theory assumed the volume fraction of coarsening particles to be infinitely small) recapture the proportionality of the rate of coarsening with the product of solubility and diffusion rate [45–47]. The coarsening of a phase which contains more than one alloying element is governed by the element with the lowest product of its solubility and diffusion rate. Thus, it is expected that, for the quaternary alloys studied, the rate of coarsening of the Q phase is proportional to the solubility of the atoms which determine the coarsening rate, *i.e.* $x_{ae}(T)$, and their diffusivity $D(T)$. The solubility $x_{ae}(T)$ of alloying atoms in the Al-rich phase often can be described by [26]

$$x_{ae}(T) = x_0 \exp\left(-\frac{\Delta H_{sol}}{kT}\right) \quad (18)$$

where ΔH_{sol} is the heat of solution of the alloying element and x_0 is a constant. The ΔH_{sol} values for Al-rich Al-Cu, Al-Mg and Al-Si binary solid solutions equal 0.42, 0.19 and 0.52 eV respectively (see refs. 48 and 49 for Al-Cu and Al-Si, while the ΔH_{sol} value for Al-Mg was obtained from solid solubility data in ref. 50). Since both $D(T)$ and $x_{\text{ae}}(T)$ have a similar exponential temperature dependence, the activation energy for the overall coarsening process will be the sum of the activation energy E_D for diffusion and the heat of solution of the alloying element, *i.e.*

$$E_A = E_D + \Delta H_{\text{sol}} \quad (19)$$

Since no solid solubility data nor diffusivity data on quaternary Al-Cu-Mg-Si alloys at the low temperature range of interest here ($T < 550$ K) are available, it is not clear which alloying element governs the time and temperature dependences of the coarsening. (Based on data for binary alloys [14], it is expected that Si is the alloying element with the lowest product of its solubility and diffusivity at temperatures below about 600 K.) Furthermore, in the quaternary system, ΔH_{sol} values obtained from the binary systems might not be valid and the activation energy for diffusion might be lowered owing to the presence of vacancies. The activation energy for Q-phase precipitation of 1.25 eV (see ref. 8) indeed hints at vacancy-enhanced diffusion. (The activation energies for volume diffusion of Cu, Mg and Si in the Al-rich phase in binary alloys are all between about 1.3 and 1.4 eV (see ref. 14).) Eventually, on the basis of the available data, the activation energy for coarsening is expected to be between about 1.4 and 1.8 eV.

In Fig. 5, the drop in hardness during overageing of ASCM alloys is given as a function of $\ln \beta$ for $E_A = 1.6$ eV. (The maximum hardnesses of ASCM0 and ASCM10 specimens are taken as 187 HV and 217 HV respectively (see Fig. 3).) Figure 5 contains data on isothermal overageing, overageing at a constant heating rate and more complex non-isothermal overageing treatments. The data points cover overageing in the temperature range from 453 to 574 K. It is observed that all the data points except two fit well to a single curve. By varying E_A , it was established that $E_A = 1.6$ eV is indeed the value for which the best-fitting single curve is obtained. This indicates that, in the temperature range considered, coarsening is the main effect causing the hardness drop during overageing. Other contributions to the hardness, such as dislocation strengthening and solid solution hardening, which are expected to increase with increasing final ageing temperature, apparently are not important.

The two points which deviate significantly from the curve in Fig. 5 concern hardness values measured after the duplex overageing treatment of heating at

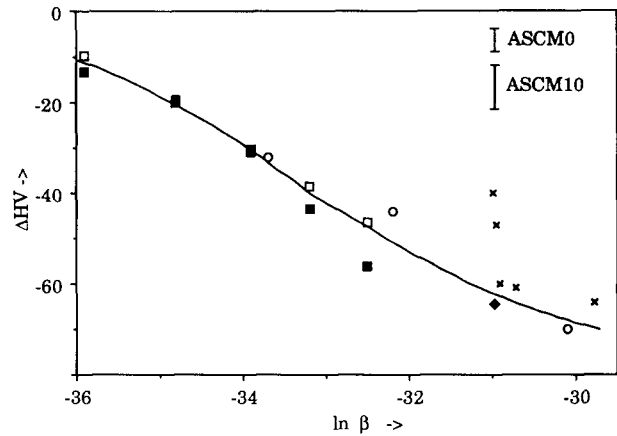


Fig. 5. Hardness drop ΔHV owing to overageing as a function of $\ln \beta$ (β in hours) for $E_A = 1.6$ eV. The data are obtained from ASCM0 specimens heated at 2 K min^{-1} to a temperature between 507 and 574 K (\circ) (see ref. 7), the same specimens, additionally aged for 100 h at 473 K (\times) [7], ASCM0 specimens aged at 453 K (\blacksquare) (Fig. 3), ASCM10 specimens aged at 453 K (\square) (Fig. 3) and ASCM0 specimens aged at temperatures below 433 K and additionally exposed for 100 h at 473 K (\blacklozenge) [7]. Typical standard deviations are indicated.

2 K min^{-1} to 487 and 507 K, respectively, followed by 100 h ageing at 473 K. An explanation for the observed deviation may be that some precipitation continues to occur during the isothermal ageing stage in these specimens.

For the application of ASCM alloy, it is noted that an optimized heat treatment consists of solution treatment at 779 K (just below the start of melting [7]), quenching and ageing for 4 h at 453 K (see Fig. 3). The solution treatment time depends on workpiece size and furnace capacity but should be as short as possible to limit coarsening of the Si particles and development of gas pores [51].

Extrapolation of the curve in Fig. 5 predicts that the hardness of a heat-treated ASCM specimen is reduced to its original as-extruded hardness (*i.e.* when $\Delta HV = -80$) when $\ln \beta = -29$ (β in hours). This corresponds, for instance, to isothermal exposure for 100 h at 500 K or isothermal exposure for 1000 h at 470 K. Hence, it is expected that, for exposures with $\ln \beta > -29$, the benefit of the heat treatment is lost. For these overageing treatments, it must be expected that the negative consequences of the solution treatment, such as coarsening of second-phase particles, grains and subgrains [41, 52], and the creation of pores owing to gas development [51], become dominant. In agreement with this, it was found recently that, after exposure for 100 h at 523 K ($\ln \beta = -27.3$), the high temperature ultimate tensile strength of the quenched and aged ASCM0 alloy is lower than that of the as-extruded ASCM0 alloy [53].

6. Conclusions

Precipitation in solid-quenched and subsequently aged specimens of Al-20at.%Si-1.5at.%Cu-1.1at.%Mg (ASCM) alloys with and without Al₂O₃ particle reinforcement was studied by X-ray diffraction and hardness measurements. The following conclusions can be drawn.

During ageing at 453 K, Q-phase precipitates first. During Q-phase precipitation, the Al-rich phase lattice parameter remains approximately constant, while the hardness increases.

After about 4 h of ageing at 453 K, θ -phase precipitation starts. During θ -phase precipitation, the Al-rich phase lattice parameter increases, while the hardness does not increase.

The presence of Al₂O₃ particles has little effect on the precipitation kinetics.

The presence of Al₂O₃ particles increases the hardness of the ASCM alloy. The increase agrees well with model predictions based on enhanced dislocation generation and reduced subgrain size owing to the presence of Al₂O₃ particles.

A model assuming the ideal plastic behaviour of the matrix describes fairly well the cooling-induced changes in the Si-rich phase lattice parameter. For the cooling-induced changes in the Al-rich phase lattice parameter, differences remain between the model predictions and measurements.

After the peak in hardness has been reached, continued ageing causes the hardness to decrease. This overageing results from coarsening of the Q-phase. The observed hardness drop as a function of temperature and time corresponds to the classical LSW coarsening theory.

An optimized heat treatment for the ASCM alloys consists of a short solution treatment at 779 K, followed by water quenching and ageing for 4 h at 453 K.

Acknowledgments

The authors are indebted to Mr. J. F. van Lent and Ing. N. M. van der Pers for assistance with the DbS experiments, and to Dr. J. Duszczyc for providing the alloys. Stimulating discussions with Prof. B. M. Korevaar, who read the manuscript critically, are gratefully acknowledged.

The financial support of the Foundation for Fundamental Research of Matter and for Technological Sciences (FOM/STW) is gratefully acknowledged.

References

- 1 D. Bialo, J. Duszczyc, A. W. J. de Gee, G. J. J. van Heijningen and B. M. Korevaar, *Wear*, 141 (1991) 291-309.
- 2 D. Bialo, T. L. J. de Haan and J. Duszczyc, *Int. Technol. Rep.*, October 1989, Delft University of Technology.
- 3 J. L. Estrada and J. Duszczyc, *J. Mater. Sci.*, 25 (1990) 886-904.
- 4 J. M. Papazian, *Metall. Trans. A*, 19 (1988) 2945-2953.
- 5 S. Abis and G. Donzelli, *J. Mater. Sci. Lett.*, 7 (1988) 51-52.
- 6 I. Dutta, S. M. Allen and J. F. Hafley, *Metall. Trans. A*, 22 (1991) 2553-2563.
- 7 M. J. Starink, V. Jooris and P. van Mourik, *Mater. Sci. For.*, 102-104 (1992) 85-97.
- 8 M. J. Starink, V. Jooris and P. van Mourik, in N. Hansen et al. (eds.), *Proc. 12th Risø Int. Symp on Metal Matrix Composites—Processing, Microstructure and Properties, Roskilde, September 2-6, 1991*, Risø, Roskilde, 1991, pp. 675-682.
- 9 H. C. Cao, M. D. Thouless and A. G. Evans, *Acta Metall.*, 36 (1988) 2037.
- 10 J. H. ter Haar and J. Duszczyc, *Mater. Sci. Eng.*, A135 (1991) 65-72.
- 11 N. A. Toropov, *CR. Acad. Sci. URSS*, 1 (1935) 147-149.
- 12 B. D. Cullity, *Elements of X-ray Diffraction*, Addison-Wesley, Reading, MA, 2nd edn., 1978.
- 13 C. J. Smithells (ed.), *Metals Reference Book*, Butterworths, London, 5th edn., 1976.
- 14 L. F. Mondolfo, *Aluminum Alloys: Structure and Properties*, Butterworths, London, 1976.
- 15 W. B. Pearson, *Handbook of Lattice Spacings and Structures of Metals and Alloys*, Vol. II, Pergamon, London, 1967.
- 16 M. J. Starink, P. van Mourik and B. M. Korevaar, *Ph.D. Thesis*, Delft University of Technology, 1992.
- 17 E. C. Ellwood, *J. Inst. Met.*, 80 (1952) 873-886.
- 18 J. E. Dorn, P. Pietrowsky and T. E. Tietz, *Trans. AIME*, 188 (1950) 933-943.
- 19 W. J. Helfrich and R. A. Dodd, *Trans. AIME*, 224 (1962) 757-762.
- 20 T. B. Massalski, in R. W. Cahn and P. Haasen (eds.), *Physical Metallurgy*, Elsevier, New York, 3rd edn., 1983, pp. 153-218.
- 21 R. B. Hill and H. J. Axon, *J. Inst. Met.*, 83 (1955) 354-356.
- 22 D. M. Poole and H. J. Axon, *J. Inst. Met.*, 80 (1952) 599-604.
- 23 R. Hamann, A. Mocellin, P.-F. Gobin and R. Fougères, *Scr. Metall. Mater.*, 26 (1992) 963-968.
- 24 W. G. Crandall, D. H. Chung and T. J. Gray, in W. W. Krieger and H. Palmour (eds.), *Mechanical Properties of Engineering Ceramics*, Wiley, New York, 1961, pp. 349-379.
- 25 W. E. Tefft, *J. Res. Nat. Bur. Stand. A*, 70 (1966) 277-280.
- 26 K. R. Van Horn (ed.), *Aluminum Properties, Physical Metallurgy and Phase Diagrams*, Vol. 1, American Society for Metals, Metals Park, OH, 1967, p. 147.
- 27 Li Shouxin, Sun Lizhi, Sue Zhengming and Wang Zhongguang, *Scr. Metall. Mater.*, 25 (1991) 2431-2434.
- 28 E. J. Mittemeijer, P. van Mourik and Th. H. de Keijser, *Philos. Mag. A*, 43 (1981) 1157-1164.
- 29 H. M. Ledbetter and M. W. Austin, *Mater. Sci. Eng.*, 89 (1987) 53-61.
- 30 M. Taya and R. J. Arsenault, *Metal Matrix Composites—Thermomechanical Behavior*, Pergamon, Oxford, 1989, pp. 106-109.
- 31 G. L. Povirk, M. G. Stout, M. Bourke, J. A. Goldstone, A. C. Lawson, M. Lovato, S. R. MacEwen, S. R. Nutt and A. Needleman, *Acta Metall. Mater.*, 40 (1992) 2391-2412.
- 32 M. Taya, K. E. Lulay and D. J. Lloyd, *Acta Metall. Mater.*, 39 (1991) 73-87.
- 33 C. T. Kim, J. K. Lee and M. R. Plichta, *Metall. Trans. A*, 21 (1990) 673-682.
- 34 R. J. Arsenault, *Scr. Metall.*, 25 (1991) 2617-2621.

- 35 R. J. Arsenault, L. Wang and C. R. Feng, *Acta Metall. Mater.*, 39 (1991) 47-57.
- 36 N. Hansen, *Acta Metall.*, 25 (1977) 863-869.
- 37 R. J. Arsenault and N. Shi, *Mater. Sci. Eng.*, 81 (1986) 175-187.
- 38 M. Taya, *Mater. Trans. JIM*, 32 (1991) 1-19.
- 39 D. C. Dunand and A. Mortensen, *Acta Metall. Mater.*, 39 (1991) 127-139.
- 40 J. R. Cahoon, W. H. Broughton and A. R. Kutzak, *Metall. Trans.*, 2 (1971) 1979-1983.
- 41 J. Zhou and J. Duszczky, *J. Mater. Sci.*, 26 (1991) 3737-3747.
- 42 H. R. Shercliff and M. F. Ashby, *Acta Metall. Mater.*, 38 (1990) 1789-1802.
- 43 I. M. Lifshitz and V. V. Slyozov, *J. Phys. Chem. Solids*, 35 (1961) 35-50.
- 44 C. Wagner, *Z. Elektrochem.*, 65 (1961) 581-591.
- 45 C. K. L. Davies, P. Nash and R. N. Stevens, *Acta Metall.*, 28 (1980) 179-189.
- 46 K. Tsumuraya and Y. Miyata, *Acta Metall.*, 31 (1983) 437-452.
- 47 P. W. Voorhees and M. E. Glicksman, *Acta Metall.*, 32 (1984) 2001-2030.
- 48 M. J. Starink and P. van Mourik, *Metall. Trans. A*, 22 (1991) 665-674.
- 49 M. van Rooyen and E. J. Mittemeijer, *Metall. Trans. A*, 20 (1989) 1207-1214.
- 50 J. L. Murray, *Bull. Alloy Phase Diag.*, 3 (1982) 60-74.
- 51 J. L. Estrada, J. Duszczky and B. M. Korevaar, *J. Mater. Sci.*, 26 (1991) 1631-1634.
- 52 J. Zhou and J. Duszczky, *J. Mater. Sci.*, 25 (1990) 4541-4548.
- 53 J. H. ter Haar and J. Duszczky, *Proc. Int. Conf. Mater. by Powder Technol.*, March 23-26, 1993, Dresden, in press.

Appendix A

To obtain the composition of the Al-rich phase after homogenizing at 779 K, we will use the Al-Cu-Mg-Si phase diagram at 775 K, as given by Mondolfo [14]. The small deviations caused by the small temperature difference will be neglected. The phase diagram shows that in the quaternary system all the Cu can be dissolved. However, some Cu is incorporated into the Al₇Cu₂Fe phase, which is observed in all the specimens by X-ray diffraction. Since the solubility of Fe in the

Al-Cu-Fe system is negligible, the entire phase is insoluble. Thus, for 1 mol of base alloy, the number of atoms in the Al₇Cu₂Fe phase is $10x_{\text{Fe}}^{\text{g}} = 0.012$ mol (where x_{Fe}^{g} is the gross Fe content of the alloy). The Mg solubility in the Al-rich phase at 775 K is about 0.65 at.%. Thus, for 1 mol of base alloy, the number x_{O} of atoms in the Q (Al₅Cu₂Mg₈Si₆) phase is $(x_{\text{Mg}}^{\text{g}} - 0.8 \times 0.0065)21/8 = 0.015$ mol (for the time being, the amount y_{a} of Al-rich phase is estimated as 0.8). The Si solubility in the Al-rich phase at 775 K is about 0.45 at.%. Thus, for 1 mol of base alloy the amount of Si phase is approximately $x_{\text{Si}}^{\text{g}} - 0.8 \times 0.0045 - (6/21)x_{\text{O}} = 0.191$ mol. The number of Cu atoms dissolved in the Al-rich phase is $x_{\text{Cu}}^{\text{g}} - 2x_{\text{Fe}}^{\text{g}} - (2/21)x_{\text{O}} = 0.0117$ mol. Now we can obtain the number of atoms in the Al-rich phase per mole of base alloy by subtracting the number of atoms in the (partially) insoluble phases from the total amount. This gives $y_{\text{a}} = 1 - 0.191 - 0.015 - 0.012 = 0.781$ mol. From this follows the estimated composition of the Al-rich phase after solid quenching: *i.e.* Al-1.5at.%Cu-0.7at.%Mg-0.5wt.%Si.

Towards the end of the applied ageing times the Al-rich phase lattice parameter reaches a stationary value. This indicates that precipitation is completed and that the composition of the Al-rich phase equals its equilibrium composition at the ageing temperature. The solubilities at the ageing temperature in the quaternary system are not known. However, all three relevant solid solubilities are expected to be very low. The solid solubility of Si in the Al-rich phase is not much affected by Cu and Mg additions. Hence, the solid solubility can be estimated from (extrapolation in) the binary Al-Si phase diagram. This solid solubility is negligibly low (about 7×10^{-5} [50]) and, thus, the Cu and Mg solid solubilities can be estimated from the ternary Al-Cu-Mg system. In the ternary Al-Cu-Mg system at 453 K, the solid solubilities obey the following rule: $x_{\text{Cu}}x_{\text{Mg}} = 1 \times 10^{-7}$ [26]. In the Al-Cu-Mg system, the sum of the two solubilities is a maximum for $x_{\text{Cu}} = x_{\text{Mg}}$, giving $x_{\text{Cu}} = x_{\text{Mg}} = 3 \times 10^{-4}$.